IEEE Access
Multidisciplinary ⋮ Rapid Review ⋮ Open Access Journal

Received 11 December 2022, accepted 8 January 2023, date of publication 16 January 2023, date of current version 23 January 2023.

*Digital Object Identifier 10.1109/ACCESS.2023.3237764*

RESEARCH ARTICLE

# A Broadband 1-Bit Single-Layer Reconfigurable Reflectarray Unit Cell Based on PIN Diode Model

**HOANG DANG CUONG[1], (Student Member, IEEE), MINH-THUY LE[2], (Member, IEEE), NGUYEN QUOC DINH[1], XUAN NAM TRAN[3], (Member, IEEE), AND NAOBUMI MICHISHITA[4], (Member, IEEE)**

[1]Faculty of Radio-Electronic Engineering, Le Quy Don Technical University, Hanoi 100000, Vietnam
[2]School of Electrical Engineering, Hanoi University of Science and Technology, Hanoi 100000, Vietnam
[3]Advanced Wireless Communication Group, Le Quy Don Technical University, Hanoi 100000, Vietnam
[4]Department of Electrical and Electronic Engineering, National Defense Academy, Yokosuka 239-0811, Japan

Corresponding author: Nguyen Quoc Dinh (dinhnq@lqdtu.edu.vn)

**ABSTRACT** Microstrip reconfigurable reflectarray antennas (RRAs) have great potential for advanced systems including satellite communications and the 6th generation (6G) wireless mobile communication networks. However, as a type of microstrip antennas, RRAs generally exhibit an intrinsic issue of narrow bandwidths. This issue is further deteriorated by complicated structures for phase shifting and DC supplying in RRAs. PIN diodes have been used in recent works to control the phases of RRA elements. However, modelling them is still costly and time consuming. In this work, a simple but novel method for modelling PIN diode SMP-1340-040 is developed by using waveguides and modified simulation approaches. Based on the obtained model, a broadband 1-bit unit cell using only one substrate is also proposed, and it achieves a simulated bandwidth of 40.6% and 33.8% for linear and circular polarizations, respectively. The experimental results show an excellent agreement with the simulation, which confirms the accuracy of the proposed PIN diode model. Moreover, the performances of the unit cell demonstrate that it can be used for designing RRAs in bands X and Ku.

**INDEX TERMS** Reflectarrays, unit cell, PIN diode model, reconfigurable antenna, linear polarization, circular polarization, broadband.

## I. INTRODUCTION

Microstrip reflectarrays (RFAs) are considered a combination of reflectors and phased array antennas with notable advantages, including affordability, light weight, and low profile with a planar structure. Compared to phased array antennas, their air-feeding mechanism avoids high loss in the feeding network. Furthermore, RFAs do not require radio frequency (RF) modules, analog-to-digital converters (ADCs), and digital-to-analog converters (DACs), rendering RFAs less complicated and more affordable than phased array antennas. Given these advantages, RFAs have been employed for satellite communications [1], [2], [3], radars, point-to-point terrestrial links, 5G [4], [5], and beyond. However, as a type of microstrip antenna, RFAs generally exhibit limited bandwidths of around 3% [6]. Recent years have witnessed significant increases in RFAs' bandwidths, elevating up to 26.7% [7], 33.52% [8] and 28.8% [9] (1-dB gain).

RRA is a variant of RFA, which can steer using phase-shifting elements. They are adopted for modern wireless communication systems with the requirement of beam steerings, such as satellite communication systems, radars, and base stations [10]. Recently, passive RIS (reconfigurable intelligent surface) or intelligent reflecting surface (IRS), which operates similarly to RRAs without horn antennas, is proposed as a promising candidate for next-generation antennas [11], [12], [13], [14]. The steering capability of RRAs is realized by devices, including MEMs (Microelectromechanical Systems), varactor diodes, PIN diodes, graphene, and liquid crystals, which tune the reflective phases of elements. Among these devices, MEMs, varactors, and PIN diodes are used more frequently. MEMs present several advantages,

The associate editor coordinating the review of this manuscript and approving it for publication was Davide Comite.

such as small size, low insertion loss, and low power consumption [15], [16], [17], [18], although fabricating them is unpopular and requires a high expense. Varactors can produce smoother reflective phases, but the expense of manufacturing a RRA with these devices is high because of the cost of the control board [19], [20], [21]. Indeed, each cell in RRAs using varactors is controlled independently by a circuit that includes a digital-to-analog converter (DAC) and some passive devices besides register shifters, microcontrollers (MCUs), or FPGAs [22], [23], which makes the control board extremely complicated and high-cost, especially when using fast-settling ADCs such as MAX5592. This problem is more critical for array with hundreds or thousands of elements which are employed for 5G [24], 6G [14], [25] and satellite [26], [27], [28], [29]. Of a particular note, PIN diodes are preferred for RRAs given their low cost, diversity, and ready availability on the market [22], [23], [30], [31], [32], [33], [34], [35], [36], [37], [38], [39], [40]. Moreover, the control boards for PIN-diode RRAs are simpler and more affordable than those for RRAs using varactors, especially for large RRAs. Most PIN-diode RRAs adopt 1 bit [22], [23], [26], [27], [30], [31], [32], [33], [39], [41], [42], [43], [44] or 2 bits [35], [36], [37] to shift reflective phases, but those using 1-bit are given more attention because of the ease of design (simple structures) [34] although their performance in terms of sidelobe levels and gains are worse (but acceptable) than those using 2 bits as a trade off.

To date, characterizing PIN diodes for RRA unit cells is still deemed a challenge, and there have been a few studies on modelling PIN diodes. Largely, PIN diode models are affected by various factors, including operating frequencies, diode mounting substrates, and controlling currents and voltages. Most types of PIN diodes have their own models provided by manufacturers; however, these models can not be applied to RRAs because they are developed under specific conditions with different substrates. Indeed, the microstrip line, which is generally used by manufacturers for the measurement of the PIN diode parameters, greatly differs from the electromagnetic conditions for the RRAs unit cell with various angles of incidence. A recent work [27] has succeeded in modelling a PIN diode by measuring a full RRA, but this method is costly and time-consuming. Another work [41] has used a waveguide to measure the reflective parameters of the RRAs unit cells; however, the method to determine the model of the PIN diodes has not been described in this literature.

The bandwidths of RRAs are affected by two factors: the structures of RRAs and the bandwidth of unit cells [6], [45]. The air-feeding structure of RRAs causes oblique effects, which deteriorate their bandwidth. This is considered an intrinsic feature of RRAs. The bandwidths of RRAs are also noticeably dependent on unit cells. Even in the cases of oblique incidences, if unit cells produced sufficiently large bandwidths, they would enlarge the bandwidths of RRAs. However, unit cells largely exhibit the narrow bandwidths which are typical for microstrip antennas. Moreover, active devices and DC-bias structures cause parasitic parameters and insertion losses, which in turn degrade the performance of unit cells considerably.

Recently, intensive effort has been made to improve the bandwidth of the RRA unit cell. In [39], a unit cell using delay lines with two PIN diodes achieved a bandwidth of 10.5%, from 13.5 GHz to 15 GHz for a phase shift of 180° ± 20°. Another unit cell formed from two patches and a PIN diode is presented in [23], which obtained a 180° ± 20° bandwidth of 12% at the center frequency of 5 GHz. Reference [43] proposed a polarization-turning element with a complicated structure, which used four layers and four PIN diodes for polarization turning, DC isolating, and impedance matching. This element operated at the center frequency of 13.25 GHz and achieved a bandwidth of nearly 20%. Reference [33] adopted a ''microstrip line-slot line-microstrip line'' structure and two PIN diodes to design a broadband unit cell. This unit cell had a bandwidth of 20.8%, from 11.6 GHz to 14.3 GHz. Because the unit cells had narrow bandwidths, RRAs achieved bandwidths still lower than RFAs, lower than 22.5% [34] compared to approximately 33.52% [8] (1- dB gain bandwidth).

Most recent works adopt multi-layer PCBs for RRAs [27], [30], [38], [39], but such structures elevate the cost of RRAs. Moreover, a multi-layer PCB uses different materials, such as PTFE and FR4 [27], [38] and some types of prepregs, which causes inhomogeneity and loss because the prepregs and FR4 typically have higher dielectric constants than PTFE [46]. This structure will also be unstable over time, resulting from the difference in thermal expansion between prepregs and other substrates [47].

In this paper, the authors focus on proposing a novel but simple method to accurately model the PIN diode. Unit cells were designed, fabricated, and tested to validate the proposed PIN diode model. Subsequently, a new structure of broadband unit cells using only one substrate and the determined PIN diode model were presented. The obtained results demonstrate that the new structure can be a viable replacement for multilayer unit cells with a number of benefits, including low cost, high stability, and reduced loss.

This paper includes four sections. Section II presents the method of modelling the PIN diode model. Section III shows the design of a broadband unit cell using the PIN model obtained in Section II and its performance. Section IV is the conclusions.

## II. PIN DIODE MODELLING

The PIN diode includes metal pads, $P_+$ and $N_+$ layers and an intrinsic region (I-region) as illustrated in Fig. 1a. The characteristics of a PIN diode mainly depend on the geometrical properties of the metal pads and the properties of the I-region. In the RRAs, PIN diodes work as a switch with two states: ''ON'' and ''OFF''. The ''ON/OFF'' states are turned when driving it by a forwarded current or supplying a reversed bias voltage, respectively. The general model of PIN diodes in these two states is outlined in Fig. 1b [48]. At the ''ON'' state, the PIN diodes are modelled as a resistor $R_{ON}$ in series with an

**TABLE 1. Parameters of the equivalent circuits of pin diode in related works.**

| Paper | PIN Diode | $L_d$ (pH) | $R_{ON}$ (Ω) | $R_{OFF}$ (Ω) | $C_d$ (fF) | Substrate | $h$ (mm) | $f_c$ (GHz) | $V_{ON/OFF}$ (V) |
|---|---|---|---|---|---|---|---|---|---|
| [31]*** | SMP-1340-040 | 450 | 1 | 10 | **126** | Arlon 880 | 0.5 | 5.35 | - |
| [27] | SMP-1340-040 | 450 | 1 | 10 | **100** | TLX-08 | 1.58 | 9.3 | 0.8; -12 |
| [36] | SMP-1340-040 | 780 | 0.8 | 10 | **202** | FR4 | 1 | 2.3 | 0.9; -0.9 |
| [49] | SMP-1340-079 | 700 | 0.78 | - | **210** | - | - | 5 | - |
| [50] | SMP-1340-079 | 700 | 0.85 | - | **210** | F4B | 3 | 8.5 | - |
| [23] | SMP-1340-040 | 450 | 1 | 10 | **160** | F4B | 2.2 | 5.0 | - |
| [39] | MADP-000907 | 30 | 7.8 | - | **25** | TLX-8 | 1.58 | 14.25 | - |
| [26] | MADP-000907 | 30 | 5.2*/7.8** | - | **40*/35**** | TLX-8 | 1.58 | 11.2/13.75 | 1.4;- |
| [32]*** | MA4AGP907 | 50 | 4.2 | 300 000 | **42** | RO4003C | 1.52 | 9.5 | - |
| [33] | MADP-000907 | 30 | 7.8 | - | **25** | Arlon AD 255C | 1.58 | 13 | - |
| [51] | MA4AGP907 | - | 4.2 | - | **20** | RT5880 | - | 12 | - |

*** The equivalent circuits for the "OFF" status of the PIN diode: $L_{OFF}$, $C_{OFF}$ and $R_{OFF}$ are paralleled. All equivalent circuits are series as Fig. 1; $h$: Thickness of the substrate diodes mounted on. *: Frequency Band: 10.0 GHz – 12.4 GHz; **: Frequency band: 12.5 GHz – 15.0 GHz.

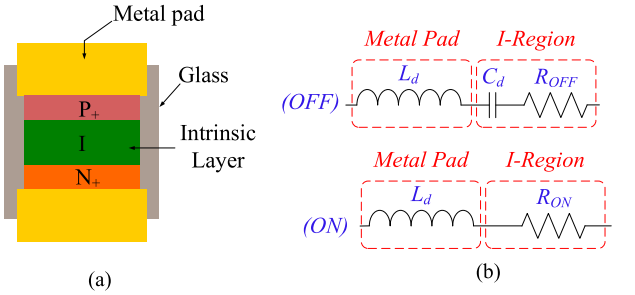


**FIGURE 1. (a) Cross section of a PIN diode; (b) The equivalent circuits of a PIN diode for both status "ON" and "OFF".**

inductor $L_d$. The $R_{ON}$ is the property of the I-region injected with holes and electrons, while the inductor $L_d$ models the metal pads [48]. The PIN diode models at the "OFF" state are described as a series of a resistor ($R_{OFF}$), a capacitor ($C_d$) and an inductor ($L_d$) where $R_{OFF}$ and $C_d$ reflect the properties of the I-region with no stored charge while $L_d$, presents the metal pads.

The PIN diode models are affected by the mounting techniques, operating frequencies, and other conditions as aforementioned. Table 1 shows the models of some kinds of PIN diodes. Most of these models are different, especially in capacitors at the "OFF" state, although some of them are the same type. Take SMP-1340-040 as an example. Its capacitor $C_d$ is adjusted from 100 fF to 202 fF, corresponding to the center frequencies from 2.3 GHz to 9 GHz. Therefore, modelling PIN diodes at their operating frequencies and substrate is necessary before designing the unit cells and RRAs.

In this work, the PIN diode SMP1340-040 from Skywork is selected for modelling. This kind of PIN diode is low cost although its characteristics are more nonlinear and lossy than MA4AGP907 and MADP-000907 from MACOM. With such a low price, SMP1340-040 is an appropriate selection for RRAs with hundreds or thousands of elements. The PIN diode SMP1340-040, with general equivalent circuits as shown in Fig. 1b, is modelled according to four steps as follows (see Fig. 2):

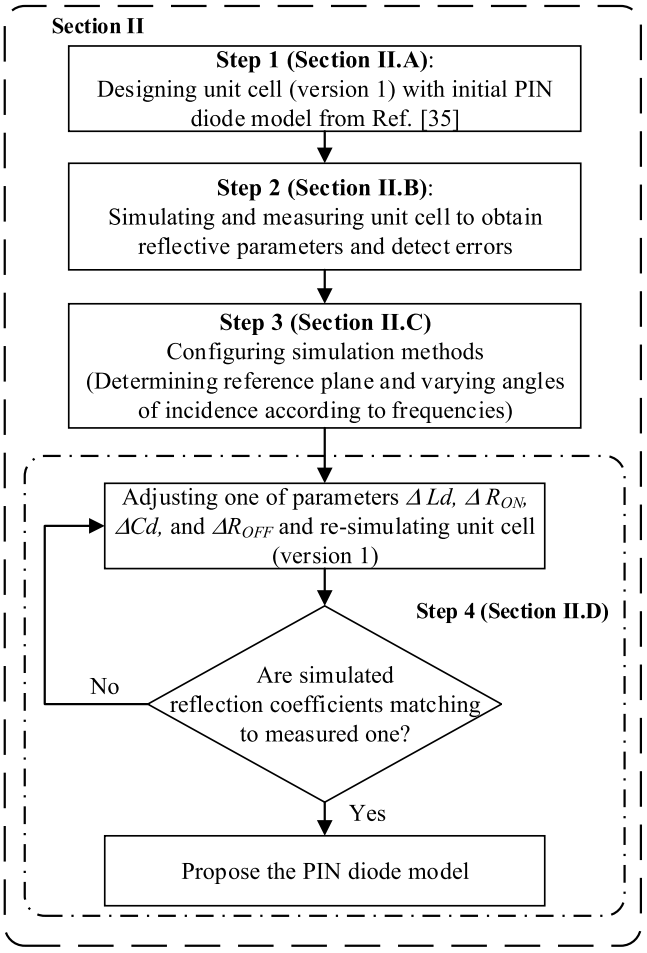


**FIGURE 2. Flow chart of the method of modelling the PIN diode.**

Step 1 (Section II-A): Design the unit cell using an initial PIN diode model extracted from [27], which operates at the center frequency of 9.2 GHz and uses substrate TLX-08 (thickness of 1.58 mm) (See Table 1). The values of the elements in the initial model are as follows: $L_d = 500$ pH, $C_d = 100$ fF, $R_{ON} = 1$ Ω, and $R_{OFF} = 10$ Ω. However, the operating conditions of the unit cell in this work are not

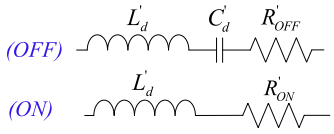


**FIGURE 3.** The real PIN diode model at both statuses "ON" and "OFF".

similar to those in [27]. Indeed, this unit cell uses a single thicker substrate and operates at frequencies from 9 GHz to 16 GHz. Therefore, the real model of the PIN diode in this paper will be different to the initial model.

Suppose that the actual PIN diode model is $L'_d$, $R'_{ON}$, $C'_d$, and $R'_{OFF}$, as illustrated in Fig. 3. Thus, the real model in relation to the initial model is expressed as follows:

$$\begin{cases} L'_d = L_d + \Delta L_d \\ R'_{ON} = R_{ON} + \Delta R_{ON} \\ C'_d = C_d + \Delta C_d \\ R'_{OFF} = R_{OFF} + \Delta R_{OFF} \end{cases} \quad (1)$$

where $\Delta L_d$, $\Delta R_{ON}$, $\Delta C_d$, and $\Delta R_{OFF}$ are adjustments of the parameters $L_d$, $R_{ON}$, $C_d$, and $R_{OFF}$ due to the different operating frequencies and substrate properties. Note that the values of these parameters can be positive (an upward adjustment) or negative (a downward adjustment).

Function (1) reveals that the errors in the model will result in differences between simulated and experimental results. However, the initial model is still used to design the unit cell because the real model is unknown.

Step 2 (Section II-B): Simulate, fabricate, and measure the unit cell designed in Step 1. In this step, the unit cell (version 1) is simulated by the periodic method with a plane wave to obtain the reflective coefficients and phases. Then, it is fabricated and measured by Keysight Vector Network Analyzer (VNA) N5242A in cooperation with a waveguide to achieve the S-parameters. The difference between experimental and simulated results is used to adjust $\Delta L_d$, $\Delta R_{ON}$, $\Delta C_d$, and $\Delta R_{OFF}$ (in Step 4). The difference between measured and simulated results mostly comes from the wrong PIN diode model and the wrong simulation method configuration. Therefore, the simulation method is configured before adjusting errors of the PIN diode models (Step 3).

Step 3 (Section II-C): Configure the simulation methods. In this section, the simulation configurations are adjusted to be analogous to the real conditions in the waveguide, where the angle of incidence is varied according to the frequencies and the reference plane is set at the surface of the unit cell.

Step 4 (Section II-D): Implement simulation-adjustment-simulation loops to obtain the PIN diode model. Errors ($\Delta L_d$, $\Delta R_{ON}$, $\Delta C_d$, and $\Delta R_{OFF}$) are adjusted gradually in loops to obtain agreements between simulated and measured reflective coefficients.

### A. UNIT CELL DESIGN

The authors use the initial PIN diode model to design the unit cell (version 1) for modelling the PIN diode. The structure

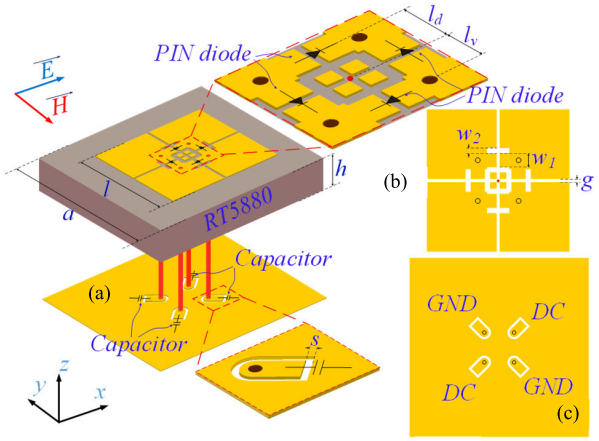


**FIGURE 4.** 3D structure of the unit cell for modelling PIN diode model: (a) 3D model, (b) top layer, and (c) bottom layer.

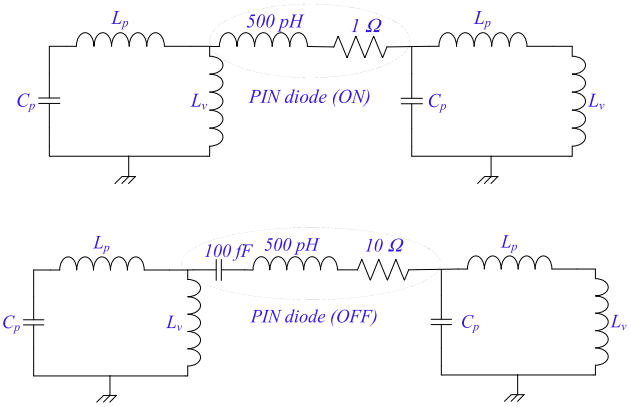


**FIGURE 5.** The equivalent circuits of the unit cell using Pin diode at the status: "ON" and "OFF".

of the unit cell is presented in Fig. 4 with dimensions of 12 mm × 12 mm, less than half of the wavelengths of the center frequency (12 GHz). Only one substrate (Duroid RT5880, $\varepsilon_r = 2.2$) with a thickness of 3.175 mm is used for the unit cell. The detailed dimensions of the structure are shown in Table 2. The unit cell has two copper layers. The top metallic layer including four rectangle patches and slots works as the main resonant component, which mostly defines the characteristics of the unit cell. Each couple of patches is connected by a PIN diode mounted on the top layer. Thus, switching states "ON" and "OFF" of four PIN diodes alters the main resonant structures of the unit cell, creating a phase shift. The slots support fixing the position of the PIN diodes. They also work as variable structures for optimizing the unit cell. The ground layer is slotted around the vias, creating four isolated patches. Two DC wires and two GND wires are soldered onto these patches to control four PIN diodes. The bottom layer is also a ground layer, working as a reflective surface. To close this surface in terms of RF signal, four 27 pF capacitors are employed to connect the four isolated patches to the remaining area, which creates a perfect

**TABLE 2. Dimensions of the unit cell for determining diode model.**

| $a$ | $l$ | $h$ | $l_d$ | $l_v$ | $g$ | $s$ | $w_1$ | $w_2$ |
|---|---|---|---|---|---|---|---|---|
| 12 | 7 | 3.175 | 1 | 1 | 0.15 | 0.15 | 0.7 | 0.25 |

Unit: mm

reflective layer. The advantage of this DC-supplying method is an excellent isolation between the DC and the RF signals, which contributes to creating a broadband unit cell.

To understand the operating principle of the unit cell more clearly, the authors model it by two equivalent circuits as illustrated in Fig. 5. Because of powerful and effective electromagnetic simulation softwares, these circuit models is used to explain the physical mechanism of the unit cells rather than optimizing or validating them [52]. For the top layer, each of the four patches is modelled as an inductor $L_p$ series with a capacitor $C_p$. Each patch is connected to the ground layer by a via to control the PIN diodes. The via is modelled as an inductor $L_v$, paralleled to the patch-modelled circuit. Each pair of patches is connected by a PIN diode and modelled by two equivalent circuits in correspondence with the "ON" and "OFF" states. Because of the direction of the electromagnetic field (see Fig. 3), the coupling between the patches in the y-axis direction is weak and could be ignored. When the PIN diodes turn "ON" or "OFF", the equivalent circuit of the unit cell is altered, respectively, which results in changing the resonant frequencies and shifting the reflective phase around 180°.

### B. SIMULATION AND MEASUREMENT

The unit cell is simulated by the periodic method with a plane wave (incident angle of 0°) in CST Studio. A couple of unit cells with dimensions of 24 mm × 12 mm are fabricated, as illustrated in Fig. 6. To mimic the walls in the simulation environment (boundary conditions), two rings of vias are employed to shut off the radiation leakage. Moreover, four holes for pinning the steel plate for solder paste printing and four holes for fixing the position of the board on the waveguide are added. Capacitors and PIN diodes are also mounted on the PCB board.

The authors intend to adopt a waveguide WR-75 to measure the unit cells, but it is not large enough to cover these double unit cells. Therefore, a couple of tapered waveguides that convert from WR75 dimensions (19.05 mm × 9.525 mm) to dimensions of 24 mm × 12 mm are designed and fabricated. They are combined with WR75 coaxial-waveguide adapters to form a set of waveguides, as illustrated in Fig. 7a. The waveguide set is calibrated by the thru-reflect-line (TRL) method [53], defining the plane of the open end (24 mm × 12 mm) of the waveguide as a reference plane. As shown in Fig. 7d, the reflection coefficient of the tapered waveguide closed by the short sheet is nearly 0 dB after calibrating, which demonstrates that the reference plane of the waveguide is calibrated. The mechanical tolerance between the two

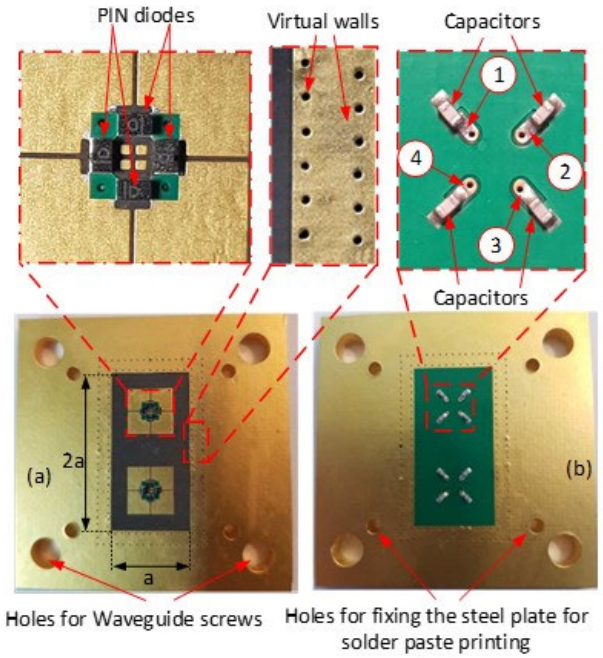


**FIGURE 6. Fabricated double unit cell: (a) top layer, and (b) bottom layer.**

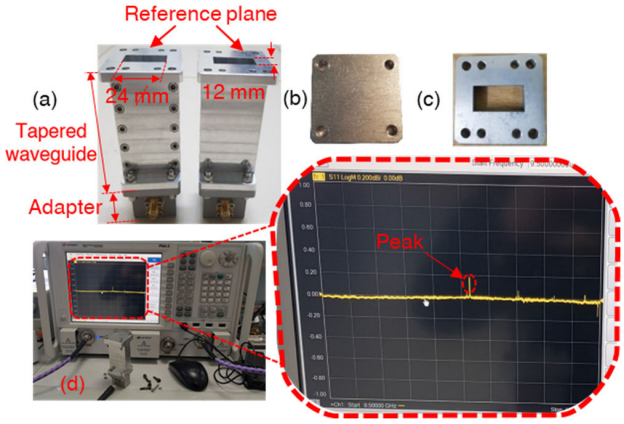


**FIGURE 7. (a) The set of tapered waveguide (two adapters and two tapers), (b) short sheet. (c) 4 wavelength delay sheet; (d) The reflection coefficient at the reference plane after calibrating.**

waveguides leads to some minor peaks of less than 0.2 dB. However, they affect the reflective parameters of the unit cell slightly.

The unit cells are placed at the reference plane to measure reflection parameters by a VNA through an RF cable (see Fig. 8) with a measurement schematic, as depicted in Fig. 9a. The unit cells are switched "ON/OFF" by a DC signal from the DC supplier. The forward current is set up by a current limiter (four resistors of 560 Ω) in cooperation with the DC supplier and is monitored by a multimeter as in Fig. 9b. Due to the similarity of the two unit cells, Fig. 9 just presents a single DC-control schematic for one unit cell as a representation. Four PIN diodes are controlled through four wires (two GND

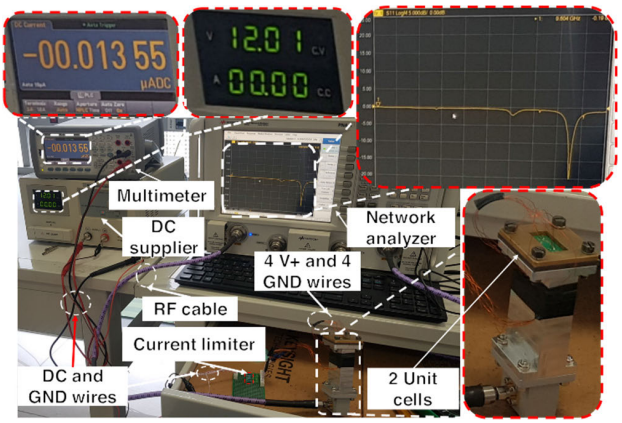


**FIGURE 8.** Measurement setup.

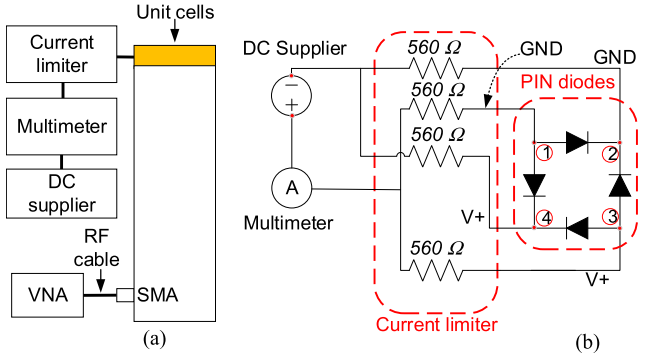


**FIGURE 9.** (a) Measurement schematic; (b) DC control schematic for each unit cell.

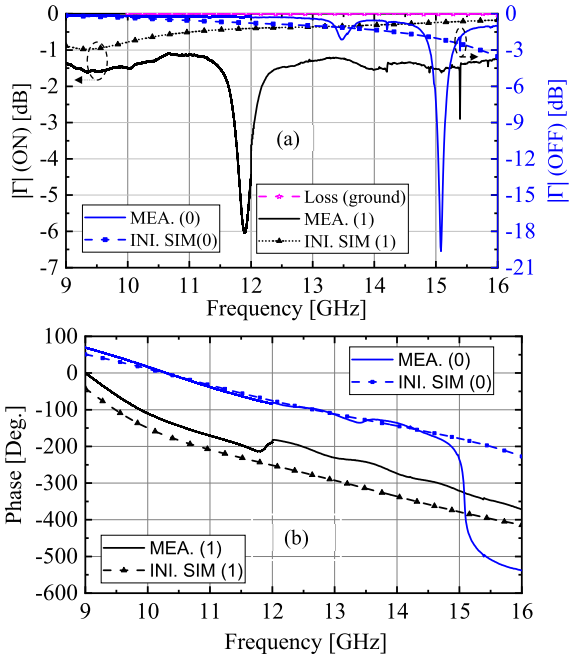


**FIGURE 10.** Simulated and measured results of unit cell with initial PIN diode model: (a) reflection coefficient, (b) reflection Phases; 1: "ON", 0: "OFF".

and two V+ wires), which connect DC signals from the current limiter to the pads 1, 2, 3, and 4 as shown in Fig. 6 and Fig. 9b. An output voltage of 6.5 V is provided to turn "ON" the PIN diodes simultaneously with a forward current of around 5 mA for each of them. A reverse voltage of −12 V is supplied to the diodes to turn them "OFF". Because the I-region in the "OFF" state (see Fig. 1) is modelled as a capacitor series to a resistor, the reverse current is nearly zero as illustrated in Fig. 8.

The measured and simulated results, as plotted in Fig. 10, are not correlated especially in reflection coefficients. For the measured reflection coefficients, there are two peaks at around 11.9 GHz for the "ON" state and two peaks at approximately 13.5 GHz and 15,1 GHz for the "OFF" state, whereas there are no peaks for the simulated results. The reflective phases also show a disagreement between measured and simulated results with deviations from 40° to 0°, especially at the "OFF" state. The simulated phase at the "OFF" state has no phase drop at 15 GHz compared to the measured one.

These errors mostly derive from the PIN diode model errors ($\Delta L_d$, $\Delta R_{ON}$, $\Delta C_d$, and $\Delta R_{OFF}$ and the incorrect simulation configuration. The errors of the PIN diode models are explained above, while simulation configuration is needed to clarify. Indeed, the current simulation configuration just uses the plane wave to excite the unit cell, which does not reflect accurately the realistic incident angle. Generally, the wave propagates in the tapered waveguide at various incident angles in correspondence with the operating frequencies. These oblique incidences excite the unit cell, creating responses greatly different from the plane wave and thus, causing errors between the simulation and the measurement. Hence, it is necessary to configure the simulation correctly and remove the errors of the diode models to match the simulated outcomes to the experimental ones.

The slotted ground layer and capacitors could affect the performance. However, this factor is excluded because the measured loss of the bottom layer is approximately 0 dB, as shown in Fig. 10a.

### C. SIMULATION METHODS

To configure the simulation conditions equivalent to the real measurement conditions correctly, the process of the electromagnetic wave travelling in the tapered waveguide has to be clarified in advance. In principle, the electromagnetic wave propagates in the waveguide at various angles $\theta$, which depend on frequency as expressed in Function (2) [54].

$$\sin(\theta) = \frac{f_{cutoff}}{f} \tag{2}$$

where $f_{cutoff}$ is the cut-off frequency of the waveguide; $f$ is the operating frequency.

The waveguide, in this case, includes two components: the waveguide adapter (WR75 adapter) and the tapered waveguide (WR75 to 24 × 12 taper), as indicated in Fig. 7. Sine the waveguide is tapered, when the wave reaches the unit cell

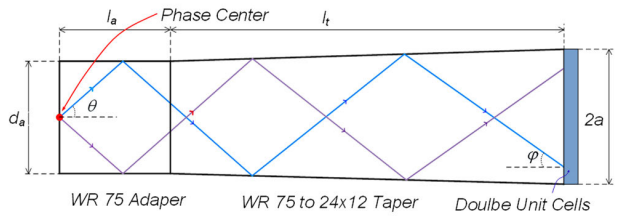


**FIGURE 11.** The process of electromagnetic wave travelling in the tapered waveguide.

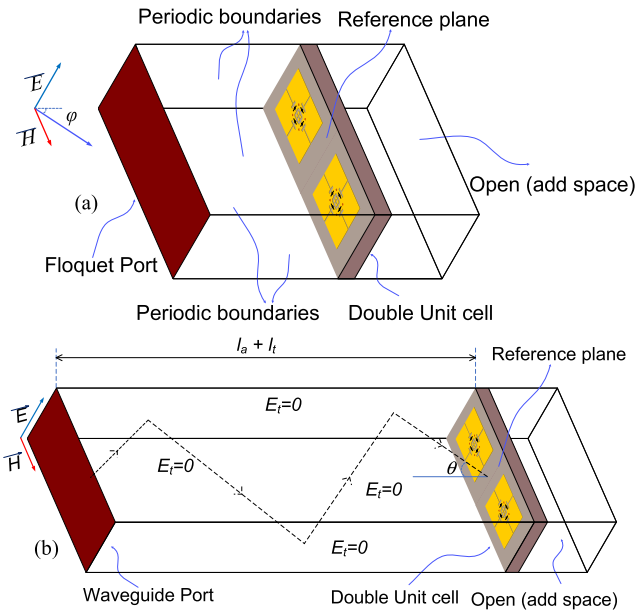


**FIGURE 12.** Simulation methods: (a) periodic method, (b) waveguide method.

surface, the incident angles $\theta$ turn into $\phi$ as shown in Fig. 11. Hence, determining the angle of incidence for each frequency is a crucial factor to simulate the unit cell accurately.

As depicted in Fig. 11, the dimensions of the whole waveguide (including the WR75 adapter) are as follows: The distance from the phase center of the adapter WR75 to its open end is $l_a = 20$ mm; The length of the tapered waveguide is $l_t = 71$ mm; The broad side dimension of the WR75 adapter is $d_a = 19.05$ mm, while that of the wider open end of the tapered waveguide is $2a = 24$ mm.

Based on the structure and the dimensions of the whole waveguide, and thanks to the geometrical method, the authors calculate a set of angles $\varphi$ for a set of discrete frequencies from 9 GHz to 16 GHz.

Both methods, namely waveguide method and periodic method, are utilized to simulate the unit cell, as depicted in Fig. 12. For the periodic method, the set of pre-calculated angles $\varphi$ are used to define the angles of incidence of the Floquet port. In contrast, the angles of incidence in the waveguide method are fixed to angles $\theta$ by the software because this method mimics a standard waveguide rather than a tapered waveguide. The length of the waveguide in the waveguide method is set to 91 mm ($l_t + l_a$), similar to the actual dimension (see Fig. 12b). The reference planes of both methods are set at the surface of the unit cell as presented in the measurement setup in Section II-B ($12 \times 24$ mm plane).

The Floquet port in the periodic method just creates a plane-wave mode, but it just slightly affects the performance of the unit cell compared to the TE10 mode in the real waveguide [52]. For the waveguide method, the boundary conditions of this method (four walls) are set to $E_t = 0$ to trigger the TE10 mode.

### D. TUNING LOOP

Due to the oblique effects, the experimental reflection coefficients have some peaks, as shown in Fig. 10, which are marks for tuning. Generally, the reactances ($L_d$ and $C_d$) of the equivalent circuit affect the frequencies of the peaks, while the resistances ($R_{ON}$ and $R_{OFF}$) just influence the peak depths. Thus, each of them is adjusted in a loop to match the experimental result to the measured one. Because the measured results are ready, the loops are just executed to tune the simulated outcomes towards the measured ones. Note that before implementing the loops, the simulation methods must be configured correctly. Since the PIN diode model at the "ON" state just has two components $L_d$ and $R_{ON}$, the loops for finding them are executed first. As shown in Fig. 13a, the measured reflection coefficient at the "ON" state just has one peak at 11.97 GHz. To determine $L'_d$, a tuning loop is implemented, in which $\Delta L_d$ is adjusted step by step to tune the frequency of the peak towards 11.97 GHz. The loop stops when the simulated frequencies of the peaks reach 11.97 GHz, with $\Delta L_d = -378$ pH and $L'_d$ ($L'_d = L_d + \Delta L_d$) $= 122$ pH. Similarly, $\Delta R_{ON}$ is adjusted in another loop to match the simulated amplitude of the peaks (11.97 GHz) to the measured one. However, due to the nonlinear characteristics of the PIN diode, the loop is terminated at $\Delta R_{ON} = 1.5\ \Omega$ ($R'_{ON} = 2.5\ \Omega$) to keep the amplitudes of all frequencies in the bandwidth close to those of the measurement. Thus, the final "ON" model is $R'_{ON} = 2.5\ \Omega$ ($\Delta R_{ON} = 1.5\ \Omega$) and $L'_d = 122$ pH ($\Delta L_d = -378$ pH).

For the "OFF" state, there are two resonant points at 13.5 GHz and 15.1 GHz, but only the peak at 15.1 GHz is considered because the other is minor, thus skipped. As depicted in Fig. 1, the parameter $L'_d$ for "ON" is the same as the "OFF" state, so it is fixed at 122 pH. Only loops for determining $C'_d$ and $R'_{OFF}$ are executed. To find $C'_d$, a loop is implemented by tuning $\Delta C_d$ gradually to move the frequency of the peak toward 15.1 GHz, and it exits when the frequency reaches that value with $\Delta C_d = 0.025$ pF. Subsequently, $\Delta R_{OFF}$ is adjusted in another loop to determine $R'_{OFF}$ and the loop stops when the amplitude of the peak at 15.1 GHz relatively matches the measured one and also keeps balanced results for other frequencies in the bandwidth with ($\Delta R_{OFF} = -5\ \Omega$). Hence, the final "OFF" model are as follows: $L'_d = 122$ pH, $C'_d = C_d + \Delta C_d = 0.125$ pF ($\Delta C_d = 0.025$ pF), $R'_{OFF} = R_{OFF} + \Delta R_{OFF} = 5\ \Omega$ ($\Delta R_{OFF} = -5\ \Omega$).

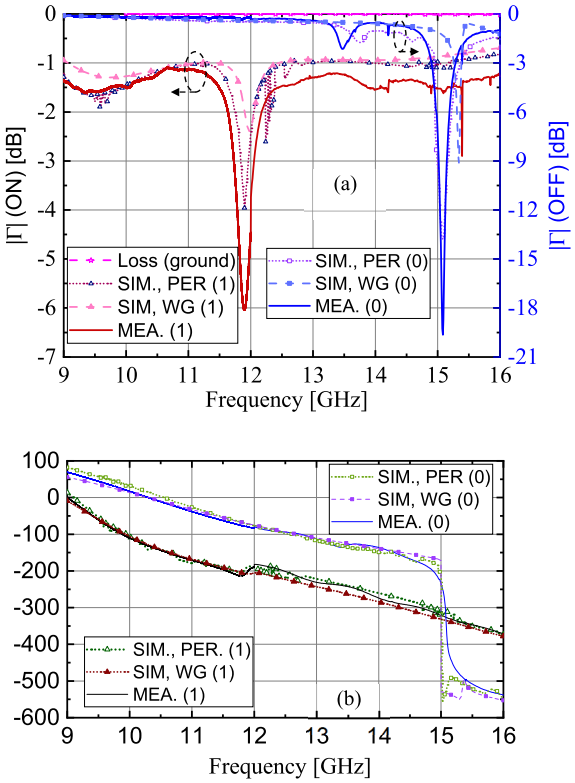


**FIGURE 13.** Simulated and measured results: (a) Reflection Coeficients. (b) Reflection phases; 1: "ON", 0: "OFF".

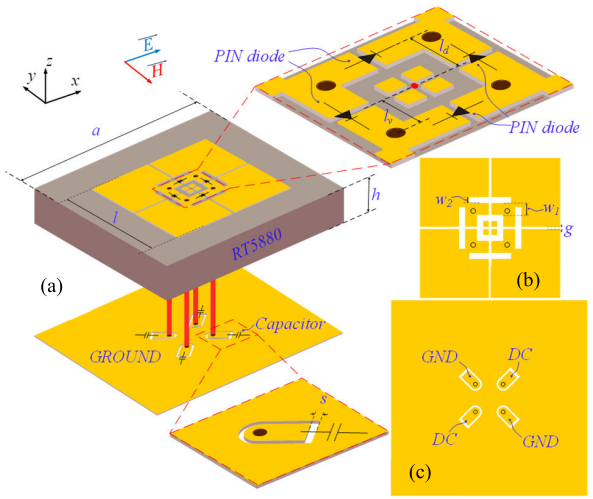


**FIGURE 14.** The structure of the broadband unit cell: (a) 3D model. (b) Top layer. (c) Bottom layer.

**TABLE 3.** Detailed dimensions of the unit cell.

| $a$ | $l$ | $h$ | $l_d$ | $l_v$ | $g$ | $s$ | $w_1$ | $w_2$ |
|---|---|---|---|---|---|---|---|---|
| 12 | 7 | 3.175 | 0.95 | 0.85 | 0.12 | 0.15 | 0.6 | 0.3 |

Unit: mm

As shown in Fig. 13b, the simulated reflective phases have an excellent agreement with those of the measurement for both simulation methods, which validates the obtained model of the PIN diode, although the phase difference does not attain 180° as expected.

Because the dimensions of the standard waveguides rarely fit the unit cell, the tapered waveguides are typically used to coordinate with VNAs for measuring unit cells. Hence, the periodic method with the set of angles of incidence is more appropriate to simulate the unit cell and obtain a better tolerance in comparison with the waveguide method.

Compared to other models of the previous works in Table 1, this model is slightly different, especially in $R'_{ON}$, $R'_{OFF}$, and $L'_d$ because the substrate, the operating frequencies, and the structure of the connecting pads are greatly different to other previous works. Regrettably, most previous works using this PIN diode do not measure unit cells. The capacitors and the gaps on the ground could be factors which affects the reflective parameters. However, the reflective characteristic of the ground layer is verified with a reflection coefficient of nearly 0 dB, as plotted in Fig. 13a, which demonstrates that it is a perfect reflective plane.

## III. BROADBAND UNIT CELL

The authors re-design the unit cell in Section II-A with the obtained PIN diode model. Parameters $l_d$, $l_v$, $g$, $w_1$ and $w_2$ are tuned to reach a phase difference of around 180° between "ON" and "OFF" states. The new structure of the proposed unit cell (version 2) is shown in Fig. 14. The detailed dimensions of the unit cell are shown in Table 3, and its operating principle is similar to the unit cell in Section II-A.

### A. UNIT CELL PERFORMANCES

The unit cell (version 2) is simulated in the periodic environment with the Floquet port, which adopts a plane wave (linear or circular polarizations) to excite the unit cell. Unlike the periodic method in Section II-C, the angle of incidence is set to zero or not changed according to the frequency. The reflection coefficients and phases of the unit cell are plotted in Fig. 15. Since the structure of the proposed unit cell is symmetric, it maintains the same linear polarizations or circular polarizations as those of the exciting sources, and its performances for x-polarized and y-polarized incidences are not significantly different. Therefore, the authors just present the simulation results for left-hand circular polarization (LHCP) and y-polarization as representations for the circular and the dual linear polarizations, respectively.

The simulated results for y-polarization are plotted in Fig. 15a and Fig. 15c, while the results for LHCP are presented in Fig. 15b and Fig. 15d. The unit cell has an excellent performance for multiple polarizations. The 180° ± 20° phase-shift bandwidth of the linear polarization is 40.6% from 9.2 GHz to 13.9 GHz, and for LHCP, it is 33.8%, from 9.26 GHz to 13.03 GHz. In these frequency ranges, the reflection coefficients for Y-polarization and LHCP are

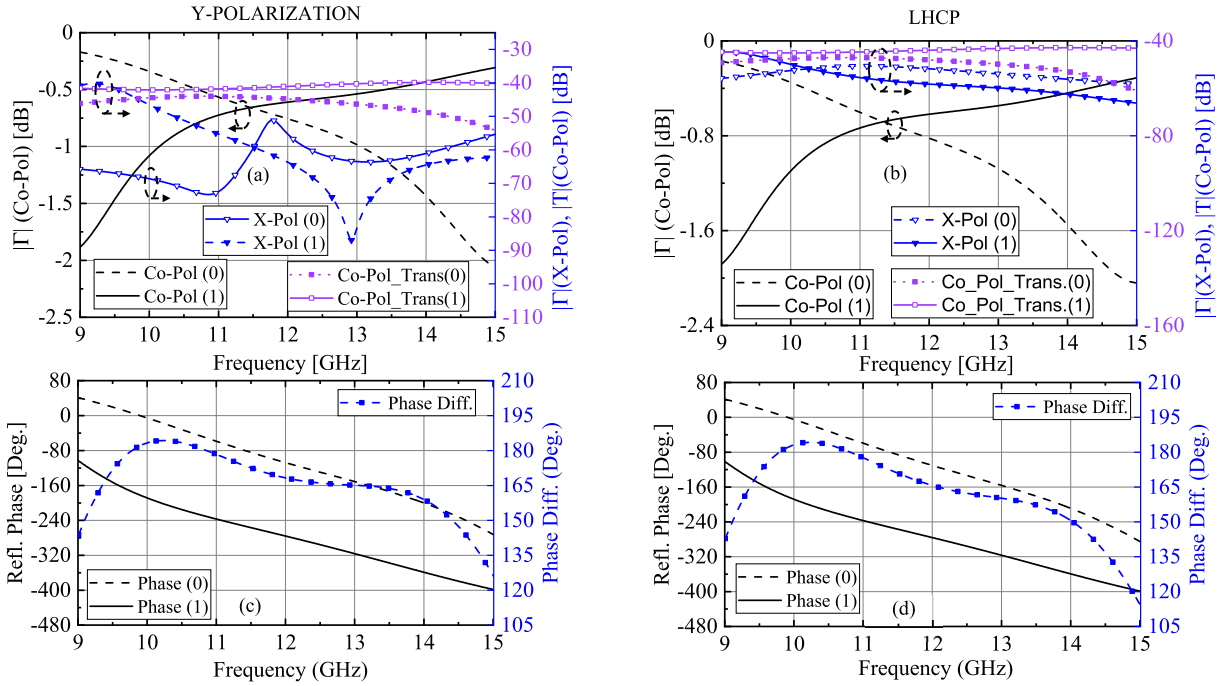


**FIGURE 15.** The simulated results: The reflection and transmission coefficients (co and cross polarization) of the unit cell for y-polarizations (a) and LHCP (b). The reflection phase of the unit cell for y-polarizations (c) and LHCP (d). 1: "ON", 0: "OFF".

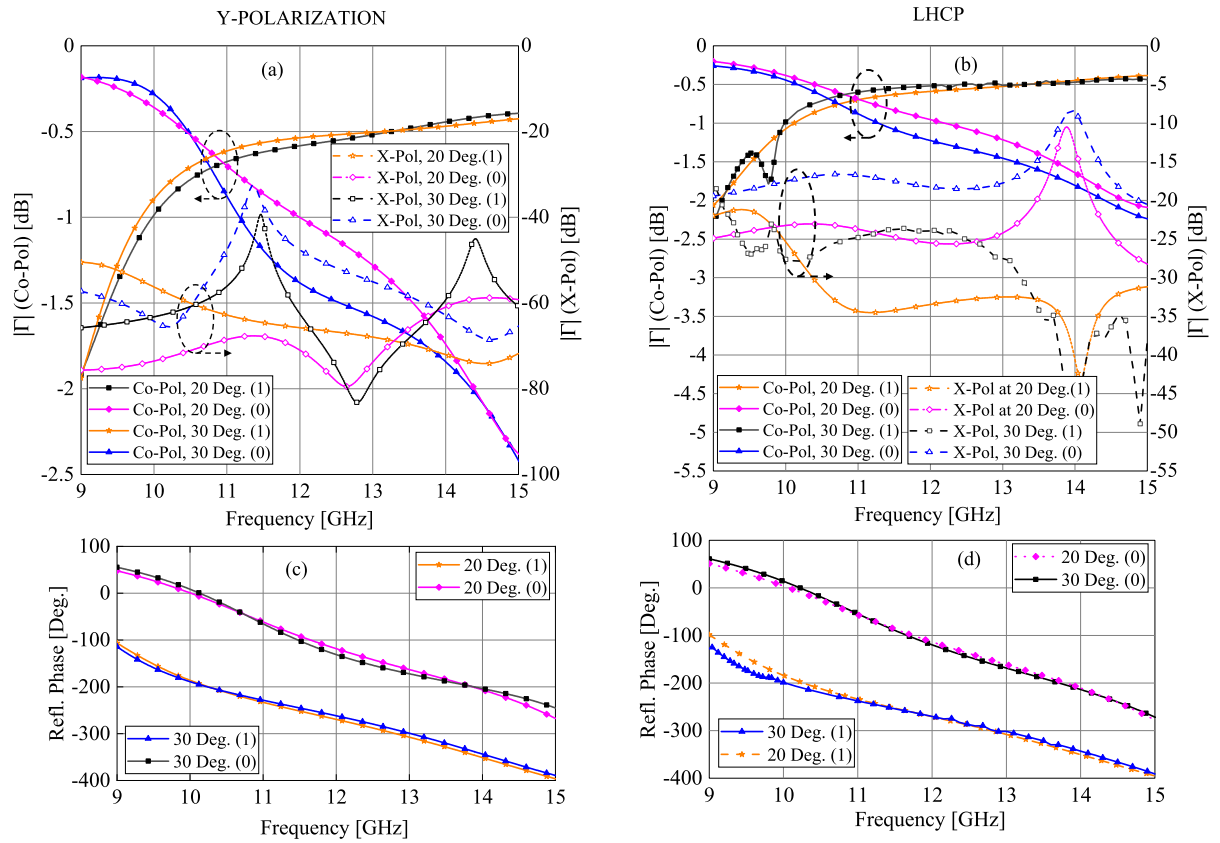


**FIGURE 16.** The simulated results in case of the oblique incidences: Reflection coefficients for Y-polarization (a) and LHCP polarization (b); Reflection phases for Y-polarization (c) and LHCP polarization (d); 1: "ON", 0: "OFF".

greater than −1.7 dB and −1.4 dB for both states "ON" and "OFF" in the bandwidths. Thus, the average reflection coefficient for both status "ON" and "OFF" is from −0.6 dB to −1 dB for both polarizations. As a result, it can

be estimated that the average radiation efficiencies of the unit cell are approximately 90% for both the "ON" and "OFF" states. The deviation of the average reflection coefficient in the bandwidths is minor (0.4 dB), which could make the unit cell a promising candidate for broadband RRAs. Moreover, the cross-polarization reflection coefficients and transmission coefficients are less than −40 dB for both Y-polarization and circular polarization. It is an excellent performance for a unit cell using such a low-cost PIN diode for frequencies up to 13.9 GHz and one layer with significantly low expense compared to a multi-layer unit cell.

This unit cell obtains a wide bandwidth because it uses a thick substrate and an appropriate structure. In fact, a shape of four patches and a thickness of 3.175 mm help the original unit cell (without PIN diodes) achieve a wideband feature because it has a more linear reflective phase [55], [56]. Four PIN diodes are placed in the middle of the unit cell to shift phase, and thus the unit cell avoids the mismatching between microstrip patches and delay lines that occurred in the previous works [22], [30]. Moreover, the proper DC-bias structures still keep the unit cell symmetrical and create an excellent isolation between DC and RF signals, while the single-layer structure also minimizes bad effects, such as nonlinear insertion loss and phase shift, compared to multi-layer structures. All of these factors contribute to creating a broadband unit cell.

Since the oblique incidence influences the performance of the unit cell significantly, it is necessary to examine the response of the unit cell at various incident angles. The simulated performances for both oblique incidences of 20° and 30° are plotted in Fig. 16. For both y-polarization and LHCP, the reflection coefficients and reflective phases at 20° and 30° show a minor deviation in comparison with the normal incidence (0°). For cross polarizations, reflection coefficients still maintain excellent isolation for Y-polarization with a figure of less than −45 dB, while for LHCP, it is less than −15 dB in the bandwidth from 9.2 GHz to 13.3 GHz. For both polarizations, the reflective phase difference between the states "ON" and "OFF" has a narrow trend from 11.5 GHz with a maximum deviation of approximately 30° for both oblique angles of 20° and 30° in comparison with the normal incidence.

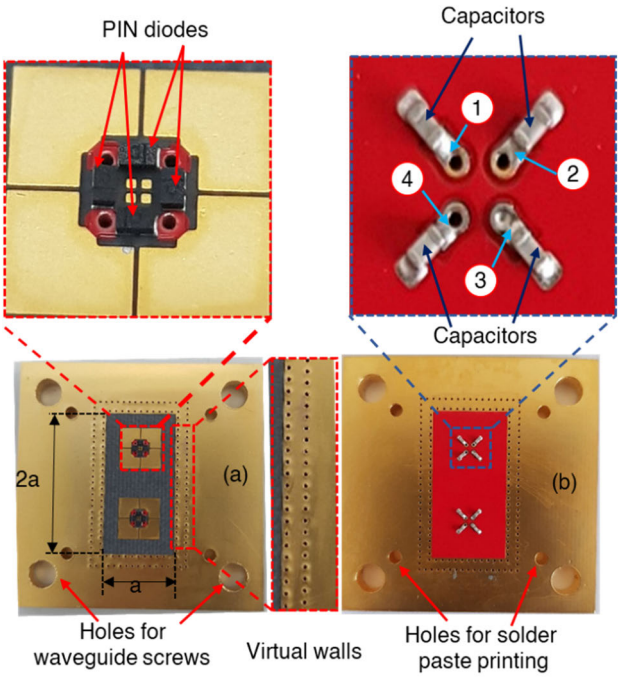


**FIGURE 17.** Fabricated broadband double cells.

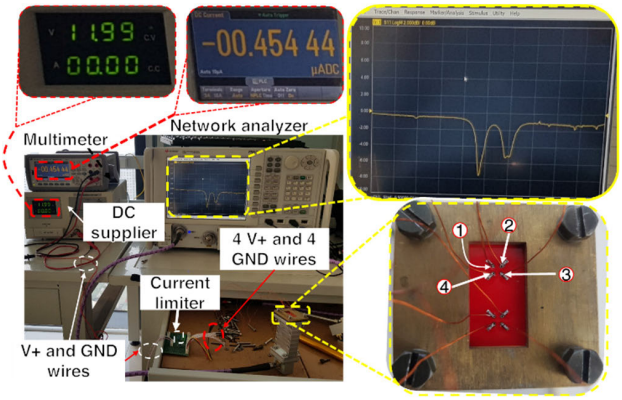


**FIGURE 18.** Measurement setup with VNA and waveguide for the broadband unit cell (version 2).

### B. FABRICATION AND MEASUREMENT

To verify the performance of the proposed structure, the double cells are fabricated. The virtual walls and holes are also employed on the board, as illustrated in Fig. 17. The unit cells are also controlled and tested as presented in Section II-B (see Fig. 18).

The measured results are compared with the simulated ones for both simulation methods (waveguide and periodic method), as shown in Fig. 19, in which the periodic method presents better errors. Indeed, for the "OFF" state, the periodic method detects a resonant point at 9.8 GHz, whereas the waveguide method ignores this point. However, there are still frequency deviations between simulated and measured peaks, particularly at 9.8 GHz with around 100 MHz, and at 12.55 GHz and 13.4 GHz with nearly 500 MHz. The errors are caused by two factors: two versions of the unit cells are fabricated at two different factories, and the PIN diode is nonlinear, especially at high frequencies. There is an excellent agreement between the simulated and measured reflection phases, as shown in Fig. 19b, which validate again the obtained PIN diode models.

Although the measured results do not reflect the characteristics of the unit cell accurately because of oblique incidences in the waveguide, the experimental phase difference of 171° to 203° for a bandwidth from 9 GHz to 13.9 GHz indicates the ability to attain a phase-shift of 180° between two states.

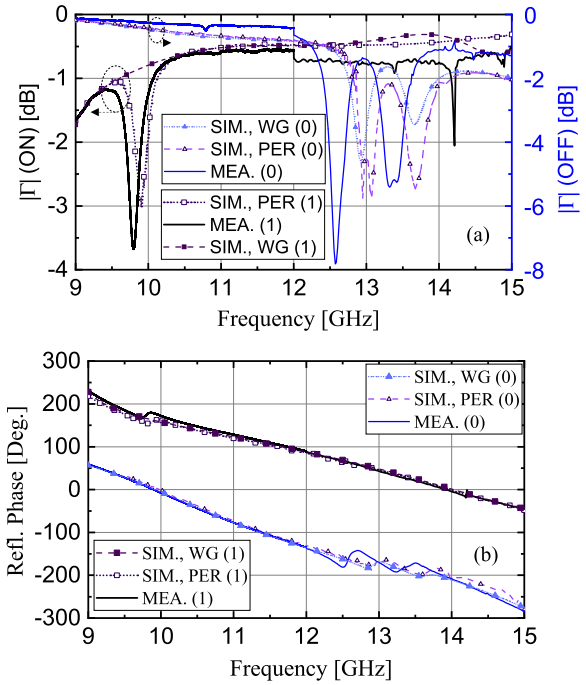


**FIGURE 19.** Measured results: (a) Reflection Coefficients; (b) Reflection Phases; 1: "ON", 0: "OFF".

**TABLE 4.** Comparison of unit cells with 1-Bit control using pin diodes.

| Ref./ Year | [43]/ 2016 | [23]/ 2019 | [33]/ 2021 | [34]/ 2022 | **This work** |
|---|---|---|---|---|---|
| f (GHz) | 12-14.5 | 4.7-5.3 | 11.6-14.3 | 12.9-16.5 | **9.2-13.9** |
| BW (%) | 18.8 | 12 | 20.8 | 23.8 | **40.6** * **33.8** ** |
| NoPD | 4 | 1 | 2 | 1 | **4** |
| PIN diode | NP | SMP | MADP | MADP | **SMP** |
| NoS | 4 | 2 | 3 | 3 | **1** |
| *h* (mm) | NP | 2.7 | 3.357 | 2.54 | **3.175** |
| \|Γ\| (dB) | -0.5 to -1 | -0.1 to -0.9 | -1.66 to -1.7 | -0.1 to -0.6 | **-0.16 to -1.7** |
| POL | DL, CP, RP | SL | SL | SL | **DL; CP** |

The common criteria for bandwidth are a phase difference of 180° ± 20° and reflective coefficients of greater than -2 dB; BW: bandwidth; NoPD: Number of PIN diodes; NoS: Number of substrates; h: the thickness of the unit cell; POL: Polarization; DL: Dual linear polarization, CP: Circular polarization; SL: Single linear polarization; *: For linear polarization; **: For circular polarization; SMP: SMP-1340-040; MADP: MADP-000907-14020.

Table 4 presents a comparison of the proposed unit cell with previous works using PIN diodes. The common criteria for determining bandwidth are a phase difference of 180°± 20° [23], [39] and reflective coefficients of greater than −2 dB. The unit cell has the greatest performance in terms of bandwidth, although it uses a low-cost diode (SMP-1340) and its structure is more simple than other works. For the reflection coefficient, due to using four diodes, the insert loss is high but acceptable, similar to [33].

## IV. CONCLUSION

This paper proposed a novel method to model a PIN diode using the periodic method for simulation and a waveguide for measurement. As a result, the model of the PIN diode SMP-1340-040 is determined. Based on this model, the authors proposed a broadband 1-bit unit cell with only one substrate layer. It achieves a wide bandwidth, from 33% to 40.6% for both polarizations, which promotes it as a promising candidate for developing a broadband RRA. The method of this work can be applied to model other PIN diodes and active devices to lower the cost of designing and fabricating RRAs.

## REFERENCES

[1] Z. Liu, X. Lei, J.-M. Wu, and Z.-J. Xu, "Dual-mode circular polarization selective surface cell for single-layer dual-band circularly polarized reflectarray," *Int. J. Antennas Propag.*, vol. 2019, Jun. 2019, Art. no. 7143274.

[2] J. Ren and W. Menzel, "Millimeter-wave single-layer dual-frequency reflectarray antenna," *Int. J. Antennas Propag.*, vol. 2017, Sep. 2017, Art. no. 6170863.

[3] S. H. Zainud-Deen, N. A. El-Shalaby, S. M. Gaber, and H. A. Malhat, "Circularly polarized transparent microstrip patch reflectarray integrated with solar cell for satellite applications," *Int. J. Microw. Sci. Technol.*, vol. 2016, Sep. 2016, Art. no. 6102530.

[4] S. Costanzo, F. Venneri, A. Borgia, and G. Di Massa, "A single-layer dual-band reflectarray cell for 5G communication systems," *Int. J. Antennas Propag.*, vol. 2019, Mar. 2019, Art. no. 9479010.

[5] H. D. Cuong, M.-T. Le, and N. Q. Dinh, "A reflectarray antenna using crosses and square rings for 5G millimeter-wave application," in *Proc. Int. Conf. Adv. Technol. Commun. (ATC)*, Nha Trang, Vietnam, Oct. 2020, pp. 126–130.

[6] J. Huang, "Bandwidth study of microstrip reflectarray and a novel phased reflectarray concept," in *Proc. IEEE Antennas Propag. Soc. Int. Symposium. Dig.*, Newport Beach, CA, USA, Jun. 1995, pp. 582–585.

[7] Y. Liu, Y. J. Cheng, X. Y. Lei, and P. F. Kou, "Millimeter-wave single-layer wideband high-gain reflectarray antenna with ability of spatial dispersion compensation," *IEEE Trans. Antennas Propag.*, vol. 66, no. 12, pp. 6862–6868, Dec. 2018.

[8] J. H. Yoon, Y. J. Yoon, W. S. Lee, and J. H. So, "Broadband microstrip reflectarray with five parallel dipole elements," *IEEE Antennas Wireless Propag. Lett.*, vol. 14, pp. 1109–1112, 2015.

[9] E.-C. Choi and S. Nam, "W-band low phase sensitivity reflectarray antennas with wideband characteristics considering the effect of angle of incidence," *IEEE Access*, vol. 8, pp. 111064–111073, 2020.

[10] S. Buzzi, E. Grossi, M. Lops, and L. Venturino, "Foundations of MIMO radar detection aided by reconfigurable intelligent surfaces," *IEEE Trans. Signal Process.*, vol. 70, pp. 1749–1763, 2022.

[11] C. You and R. Zhang, "Wireless communication aided by intelligent reflecting surface: Active or passive?" *IEEE Wireless Commun. Lett.*, vol. 10, no. 12, pp. 2659–2663, Dec. 2021.

[12] E. Basar, M. Di Renzo, J. De Rosny, M. Debbah, M. Alouini, and R. Zhang, "Wireless communications through reconfigurable intelligent surfaces," *IEEE Access*, vol. 7, pp. 116753–116773, 2019.

[13] Y. Liu, S. Zhang, X. Mu, Z. Ding, R. Schober, N. Al-Dhahir, E. Hossain, and X. Shen, "Evolution of NOMA toward next generation multiple access (NGMA) for 6G," *IEEE J. Sel. Areas Commun.*, vol. 40, no. 4, pp. 1037–1071, Apr. 2022.

[14] Z. Zhang, L. Dai, X. Chen, C. Liu, F. Yang, R. Schober, and H. V. Poor, "Active RIS vs. passive RIS: Which will prevail in 6G?" *IEEE Trans. Commun.*, early access, Dec. 23, 2022, doi: 10.1109/TCOMM.2022.3231893.

[15] S. Montori, E. Chiuppesi, P. Farinelli, L. Marcaccioli, R. V. Gatti, and R. Sorrentino, "W-band beam-steerable MEMS-based reflectarray," *Int. J. Microw. Wireless Technol.*, vol. 3, no. 5, pp. 521–532, Sep. 2011.

[16] T. Debogovic and J. Perruisseau-Carrier, "Low loss MEMS-reconfigurable 1-bit reflectarray cell with dual-linear polarization," *IEEE Trans. Antennas Propag.*, vol. 62, no. 10, pp. 5055–5060, Oct. 2014.

[17] S. Montori, L. Marcaccioli, R. V. Gatti, and R. Sorrentino, "Constant-phase dual polarization MEMS-based elementary cell for electronic steerable reflectarrays," in *Proc. Eur. Microw. Conf. (EuMC)*, Rome, Italy, Sep. 2009, pp. 033–036.

[18] O. Bayraktar, O. A. Civi, and T. Akin, "Beam switching reflectarray monolithically integrated with RF MEMS switches," *IEEE Trans. Antennas Propag.*, vol. 60, no. 2, pp. 854–862, Feb. 2012.

[19] S. Costanzo, F. Venneri, A. Raffo, and G. Di Massa, "Dual-layer single-varactor driven reflectarray cell for broad-band beam-steering and frequency tunable applications," *IEEE Access*, vol. 6, pp. 71793–71800, 2018.

[20] F. Venneri, S. Costanzo, and G. Di Massa, "Design and validation of a reconfigurable single varactor-tuned reflectarray," *IEEE Trans. Antennas Propag.*, vol. 61, no. 2, pp. 635–645, Feb. 2013.

[21] M. E. Trampler, R. E. Lovato, and X. Gong, "Dual-resonance continuously beam-scanning *X*-band reflectarray antenna," *IEEE Trans. Antennas Propag.*, vol. 68, no. 8, pp. 6080–6087, Aug. 2020.

[22] H. Yang, F. Yang, S. Xu, Y. Mao, M. Li, X. Cao, and J. Gao, "A 1-bit $10 \times 10$ reconfigurable reflectarray antenna: Design, optimization, and experiment," *IEEE Trans. Antennas Propag.*, vol. 64, no. 6, pp. 2246–2254, Jun. 2016.

[23] J. Han, L. Li, G. Liu, Z. Wu, and Y. Shi, "A wideband 1 bit $12 \times 12$ reconfigurable beam-scanning reflectarray: Design, fabrication, and measurement," *IEEE Antennas Wireless Propag. Lett.*, vol. 18, no. 6, pp. 1268–1272, Jun. 2019.

[24] J. He, F. Jiang, K. Keykhosravi, J. Kokkoniemi, H. Wymeersch, and M. Juntti, "Beyond 5G RIS mmWave systems: Where communication and localization meet," *IEEE Access*, vol. 10, pp. 68075–68084, 2022.

[25] M. Z. Chowdhury, M. Shahjalal, S. Ahmed, and Y. M. Jang, "6G wireless communication systems: Applications, requirements, technologies, challenges, and research directions," *IEEE Open J. Commun. Soc.*, vol. 1, pp. 957–975, 2020.

[26] H. Yang, F. Yang, X. Cao, S. Xu, J. Gao, X. Chen, M. Li, and T. Li, "A 1600-element dual-frequency electronically reconfigurable reflectarray at X/Ku-band," *IEEE Trans. Antennas Propag.*, vol. 65, no. 6, pp. 3024–3032, Jun. 2017.

[27] X. Pan, F. Yang, S. Xu, and M. Li, "A 10 240-element reconfigurable reflectarray with fast steerable monopulse patterns," *IEEE Trans. Antennas Propag.*, vol. 69, no. 1, pp. 173–181, Jan. 2021.

[28] P. Angeletti and R. De Gaudenzi, "A pragmatic approach to massive MIMO for broadband communication satellites," *IEEE Access*, vol. 8, pp. 132212–132236, 2020.

[29] L. You, K.-X. Li, J. Wang, X. Gao, X.-G. Xia, and B. Ottersten, "Massive MIMO transmission for LEO satellite communications," *IEEE J. Sel. Areas Commun.*, vol. 38, no. 8, pp. 1851–1865, Aug. 2020.

[30] H. Kamoda, T. Iwasaki, J. Tsumochi, T. Kuki, and O. Hashimoto, "60-GHz electronically reconfigurable large reflectarray using single-bit phase shifters," *IEEE Trans. Antennas Propag.*, vol. 59, no. 7, pp. 2524–2531, Jul. 2011.

[31] M. Wang, S. Xu, F. Yang, and M. Li, "A 1-bit bidirectional reconfigurable transmit-reflect-array using a single-layer slot element with PIN diodes," *IEEE Trans. Antennas Propag.*, vol. 67, no. 9, pp. 6205–6210, Sep. 2019.

[32] F. Wu, R. Lu, J. Wang, Z. H. Jiang, W. Hong, and K.-M. Luk, "A circularly polarized 1 bit electronically reconfigurable reflectarray based on electromagnetic element rotation," *IEEE Trans. Antennas Propag.*, vol. 69, no. 9, pp. 5585–5595, Sep. 2021.

[33] B. Xi, Y. Xiao, K. Zhu, Y. Liu, H. Sun, and Z. Chen, "1-bit wideband reconfigurable reflectarray design in Ku-band," *IEEE Access*, vol. 10, pp. 4340–4348, 2022.

[34] S.-G. Zhou, G. Zhao, H. Xu, C.-W. Luo, J.-Q. Sun, G.-T. Chen, and Y.-C. Jiao, "A wideband 1-bit reconfigurable reflectarray antenna at *Ku*-band," *IEEE Antennas Wireless Propag. Lett.*, vol. 21, no. 3, pp. 566–570, Dec. 2021.

[35] R. Pereira, R. Gillard, R. Sauleau, P. Potier, T. Dousset, and X. Delestre, "Dual linearly-polarized unit-cells with nearly 2-bit resolution for reflectarray applications in X-band," *IEEE Trans. Antennas Propag.*, vol. 60, no. 12, pp. 6042–6048, Dec. 2012.

[36] L. Dai, B. Wang, M. Wang, X. Yang, J. Tan, S. Bi, S. Xu, F. Yang, Z. Chen, and M. Di Renzo, "Reconfigurable intelligent surface-based wireless communications: Antenna design, prototyping, and experimental results," *IEEE Access*, vol. 8, pp. 45913–45923, 2020.

[37] B. D. Nguyen, V.-S. Tran, L. Mai, and P. Dinh-Hoang, "A two-bit reflectarray element using cut-ring patch coupled to delay lines," *REV J. Electron. Commun.*, vol. 6, no. 1–2, pp. 30–34, Mar. 2016.

[38] H. Zhang, X. Chen, Z. Wang, Y. Ge, and J. Pu, "A 1-bit electronically reconfigurable reflectarray antenna in X band," *IEEE Access*, vol. 7, pp. 66567–66575, 2019.

[39] H. Yang, F. Yang, S. Xu, M. Li, X. Cao, and J. Gao, "A 1-bit multipolarization reflectarray element for reconfigurable large-aperture antennas," *IEEE Antennas Wireless Propag. Lett.*, vol. 16, pp. 581–584, 2016.

[40] S. V. Hum, M. Okoniewski, and R. J. Davies, "Modeling and design of electronically tunable reflectarrays," *IEEE Trans. Antennas Propag.*, vol. 55, no. 8, pp. 2200–2210, Aug. 2007.

[41] A. Clemente, L. Dussopt, R. Sauleau, P. Potier, and P. Pouliguen, "1-bit reconfigurable unit cell based on PIN diodes for transmit-array applications in *X*-band," *IEEE Trans. Antennas Propag.*, vol. 60, no. 5, pp. 2260–2269, May 2012.

[42] L. Di Palma, A. Clemente, L. Dussopt, R. Sauleau, P. Potier, and P. Pouliguen, "1-bit reconfigurable unit cell for Ka-band transmitarrays," *IEEE Antennas Wireless Propag. Lett.*, vol. 15, pp. 560–563, 2016.

[43] M.-T. Zhang, S. Gao, Y.-C. Jiao, J.-X. Wan, B.-N. Tian, C.-B. Wu, and A.-J. Farrall, "Design of novel reconfigurable reflectarrays with single-bit phase resolution for Ku-band satellite antenna applications," *IEEE Trans. Antennas Propag.*, vol. 64, no. 5, pp. 1634–1641, May 2016.

[44] X. Pan, F. Yang, S. Xu, and M. Li, "Mode analysis of 1-bit reflectarray element using p-i-n diode at W-band," in *Proc. IEEE Int. Symp. Antennas Propag. USNC/URSI Nat. Radio Sci. Meeting*, San Diego, CA, USA, Jul. 2017, pp. 2055–2056.

[45] D. M. Pozar, "Bandwidth of reflectarrays," *Electron. Lett.*, vol. 39, no. 21, pp. 1490–1491, Oct. 2003.

[46] V. Weis. (1997.) *Combining Dielectrics in Multilayer Microwave Boards*. Rogers Corporation. Bear, DE, USA. Accessed: Jul. 10, 2022. [Online]. Available: https://imageserv11.team-logic.com/mediaLibrary/303/Combining_Dielectrics_05_20_13.pdf

[47] R. R. Hornung and J. C. Frankosky, "Microwave laminate material considerations for multilayer applications," in *Proc. Eur. Microw. Conf.*, 2007, pp. 1425–1428.

[48] *The PIN Diode Circuit Designers' Handbook*, Microsemi Corporation, Santa Ana, CA, USA, 1998, pp. 3–4.

[49] C.-W. Luo, G. Zhao, Y.-C. Jiao, G.-T. Chen, and Y.-D. Yan, "Wideband 1 bit reconfigurable transmitarray antenna based on polarization rotation element," *IEEE Antennas Wireless Propag. Lett.*, vol. 20, no. 5, pp. 798–802, May 2021.

[50] C.-W. Luo, Y.-C. Jiao, G.-T. Chen, and G. Zhao, "Reconfigurable slot coupling reflectarray," in *Proc. Int. Symp. Antennas Propag. (ISAP)*, Xi'an, China, 2019, pp. 1–3.

[51] B. D. Nguyen and S. V. Tran, "Beam-steering reflectarray based on two-bit aperture-coupled reflectarray element," *J. Electromagn. Waves Appl.*, vol. 32, no. 1, pp. 54–66, Jan. 2018.

[52] P. Nayeri, F. Yang, and A. Z. Elsherbeni, "Analysis and design of reflectarray elements," in *Reflectarray Antennas: Theory, Designs and Applications*. Hoboken, NJ, USA: Wiley-IEEE Press, 2018, pp. 86–87.

[53] V. Niculae and U. Pisani, "TRL calibration kit for characterizing waveguide-embedded microstrip circuits at millimeter-wave frequencies," in *Proc. 19th IEEE Instrum. Meas. Technol. Conf.*, Anchorage, AK, USA, Mar. 2002, pp. 1349–1354.

[54] G. L. Ragan, "Element line theory," in *Microwave Transmission Circuits*, L. N. Ridenour, Ed. New York, NY, USA: McGraw-Hill Book Company, 1948, pp. 46–47.

[55] M. R. Chaharmir, J. Shaker, M. Cuhaci, and A. Ittipiboon, "A broadband reflectarray antenna with double square rings," *Microw. Opt. Technol. Lett.*, vol. 48, no. 7, pp. 1317–1320, Jul. 2006.

[56] M. R. Chaharmir, J. Shaker, M. Cuhaci, and A. Ittipiboon, "Broadband reflectarray antenna with double cross loops," *Electron. Lett.*, vol. 42, no. 2, pp. 65–66, Jan. 2006.

**HOANG DANG CUONG** (Student Member, IEEE) received the B.E. degree in electrical engineering from Le Quy Don Technical University, in 2005, and the M.S. degree in electronic engineering from the Ho Chi Minh City University of Technology, in 2013. He is currently pursuing the Ph.D. degree in electronic engineering with Le Quy Don Technical University. His research interests include embedded systems, beamforming, metamaterials, reflectarray antennas, reconfigurable reflectarray antennas, and microwave circuits.

**MINH-THUY LE** (Member, IEEE) was born in Vietnam. She received the B.E. and M.S. degrees in electrical engineering from the Hanoi University of Science and Technology (HUST), in 2006 and 2008, respectively, and the Ph.D. degree in optics and radio frequency from the Grenoble Institute of Technology, France, in 2013. She is currently a Lecturer and the Group Leader of the Radio Frequency Group, Department of Instrumentation and Industrial Informatics (3I), School of Electrical Engineering (SEE), HUST. Her current research interests include built-in antenna, antenna array, beamforming, metamaterials, indoor localization and RF energy harvesting, wireless power transfer, and autonomous wireless sensor.

**NGUYEN QUOC DINH** received the B.E., M.E., and D.E. degrees from the Department of Electrical and Electronic Engineering, National Defense Academy, Yokosuka, Japan, in 2006, 2008, and 2011, respectively. Since 2011, he has been a Research Associate with the Faculty of Radio-Electronics Engineering, Le Quy Don Technical University, Hanoi, Vietnam, where he is currently an Associate Professor. His research interests include very small antennas, array antennas, UWB antennas, and MIMO antennas. He is a member of the Institute of Electronics, Information and Communication Engineers (IEICE), Japan. He was a recipient of the Young Scientist Award from the IEICE Antennas and Propagation Society Japan Chapter, Japan, in 2011.

**XUAN NAM TRAN** (Member, IEEE) received the M.E. degree in telecommunications engineering from the University of Technology Sydney, Australia, in 1998, and the D.Eng. degree in electronic engineering from The University of Electro-Communications, Japan, in 2003. From November 2003 to March 2006, he was a Research Associate at the Information and Communication Systems Group, Department of Information and Communication Engineering, The University of Electro-Communications. He is currently a Full Professor and the Head of the Strong Research Group on Advanced Wireless Communications, Le Quy Don Technical University. His research interests include space-time signal processing for communications, such as adaptive antennas, space-time coding, MIMO, spatial modulation, and cooperative communications. He is a member of IEICE and the Radio-Electronics Association of Vietnam (REV). He was a recipient of the 2003 IEEE AP-S Japan Chapter Young Engineer Award and a co-recipient of the two Best Paper Awards from the 2012 International Conference on Advanced Technologies for Communications and the 2014 National Conference on Electronics, Communications and Information Technology. He is the Founding Chair and the Chapter Chair of the Vietnam Chapter of IEEE Communications Society.

**NAOBUMI MICHISHITA** (Member, IEEE) received the B.E., M.E., and D.E. degrees in electrical and computer engineering from Yokohama National University, Yokohama, Japan, in 1999, 2001, and 2004, respectively. In 2004, he was a Research Associate at the Department of Electrical and Electronic Engineering, National Defense Academy, Kanagawa, Japan, where he is currently a Professor. From 2006 to 2007, he was a Visiting Scholar at the University of California at Los Angeles, Los Angeles, CA, USA. His current research interests include metamaterial antenna and electromagnetic analysis. He is a Senior Member of the Institute of Electronics, Information and Communication Engineers (IEICE), Japan. He is also a member of the Japan Society for Simulation Technology. He was a recipient of the Young Engineer Award presented by the IEEE Antennas and Propagation Society Japan Chapter and the IEICE, Japan, in 2004 and 2005, respectively. He received the Best Paper Award and the Best Tutorial Paper Award from the IEICE Communication Society, in 2013 and 2014, respectively. He received the 32nd Radio Achievement Award by the Association of Radio Industries and Businesses, in 2021, for the development of an optically transparent dual-band meta-surface reflector. He has been serving as a Secretary of the Technical Committee on Antennas and Propagation of the IEICE, since 2021.